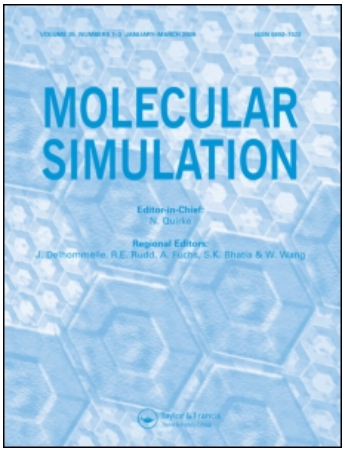

Molecular Simulation
Publication details, including instructions for authors and subscription information:
http://www.informaworld.com/smpp/title~content=t713644482

Influence of Cooperativity on Hydrogen Bond Networks

Michel Masella[a]; Jean-Pierre Flament[b]
[a] Service de Biochimie et de Biologie Moléculaire de l'Hôpital Lariboisière, Paris Cedex 10, France [b] Laboratoire de physique des lasers, atomes et molecules, CNRS (UMR 8523), Centre d'Etude et de Recherche Lasers et Applications, Université de Lille-1, Villeneuve d'Ascq Cedex, France

To cite this Article Masella, Michel and Flament, Jean-Pierre(2000) 'Influence of Cooperativity on Hydrogen Bond Networks', Molecular Simulation, 24: 1, 131 — 156
To link to this Article: DOI: 10.1080/08927020008024192
URL: http://dx.doi.org/10.1080/08927020008024192

Molecular Simulation, 2000, Vol. 24, pp. 131–156
Reprints available directly from the publisher
Photocopying permitted by license only

INFLUENCE OF COOPERATIVITY ON HYDROGEN BOND NETWORKS

MICHEL MASELLA[a,*] and JEAN-PIERRE FLAMENT[b]

[a]*Service de Biochimie et de Biologie Moléculaire de l'Hôpital Lariboisière, CR C. Bernard, IFR 6, 2 rue Ambroise Paré, 75475 Paris Cedex 10, France;* [b]*Laboratoire de physique des lasers, atomes et molecules, CNRS (UMR 8523), Centre d'Etude et de Recherche Lasers et Applications, Université de Lille-1, Bâtiment P5, 59655 Villeneuve d'Ascq Cedex, France*

(Received April 1999; accepted May 1999)

Cooperative effects are known to strongly affect the geometrical, energetic and vibrational properties of hydrogen bonded systems. In particular, such effects strongly favor molecular arrangements where each molecule is simultaneously a donor and an acceptor of hydrogen bonds (HBs), regardless of the chemical nature of the monomer subunits. In the particular case of water systems, it has been shown that the more a molecule is a proton donor in HBs, the more the HBs where it is a proton acceptor are reinforced. Such a property could be at the origin of the equilibrium between the two species of hydrogen bonded water molecules in liquid water (one with a strong hydrogen bonding character, and one with a weaker one), as experimentally evidenced and as a molecular dynamic study of the small $(H_2O)_{24}$ cluster clearly suggests.

Keywords: Hydrogen bonds; cooperativity; clusters

1. COOPERATIVE EFFECTS AND HYDROGEN BONDED SYSTEMS

Hydrogen bonding corresponds to a weak interaction (less than 10 kcal mol^{-1} per hydrogen bond, HB) involving usually two electronegative atoms and a hydrogen with the pattern X-H—Y (however, recently, H—H HBs have been proposed [1]). This interaction is characterized by a strong directionality (usually the X-H—Y angle has to be close to 180°). This

*Corresponding author.

interaction is fundamental in biochemistry (in particular, to understand the properties of proteins, DNA, *etc.*, supress) and also in many fields of physical-chemistry because of the fundamental role played by water on earth. However, because of the weakness of this interaction, it has until recently been difficult to experimentally observe small isolated hydrogen bonded clusters, and, therefore, to test theoretical hypotheses regarding the properties of this interaction. In the particular case of water clusters, using infrared and far-infrared spectrometry techniques, it has been recently possible to observe and to characterize the structural and vibrational properties of small water clusters from 2 to 8 molecules [2–4], and several theoretical studies have been devoted to them to interpret the experimental results. Other types of HB clusters have been also experimentally investigated (such as the NH_3 homo and (CH_2O, H_2O) hetero dimers [5, 6]). However, the greatest efforts were devoted to water systems, and, by comparing experimental results to theoretical studies, it has appeared that many-body effects strongly affect the geometrical, vibrational and energetic properties of water clusters, and, therefore, they have to be accounted for to thoroughly describe larger water systems. In the following sections, cooperative effects correspond to the sum of all of the many-body contributions greater than the second order, defined as follows:

$$\mathrm{BE} = \sum_{i,j} \Delta E_{ij} + \underbrace{\sum_{i,j,k} \Delta E_{ijk} + \sum_{i,j,k,l} \Delta E_{ijkl} + \cdots}_{\text{Cooperative effects}} \tag{1}$$

In Eq. (1), BE corresponds to the cluster binding energy and ΔE_{ij} to interactions between each dimer subunit of the cluster.

2. COOPERATIVE EFFECTS IN SMALL HYDROGEN BONDED CLUSTERS

2.1. Theoretical Difficulty in Describing Hydrogen Bonded Systems

To theoretically characterize the properties of chemical systems, quantum computational methods (in particular, the *ab initio* ones) are the most accurate. However, the description of HB systems needs a high level of theory which is highly computationaòl expensive. In particular, it has been shown that electronic correlation effects have to be accounted for (using, for instance, MPx methods, $x = 2 - 4$) and very extended and flexible basis sets

have to be considered during the computations [7]. However, even using very extended basis sets, the basis set superposition error (BSSE) remains large. In the particular case of the water dimer, even using the 6 – 311 + G(2df, 2p) basis set (representing about hundred orbitals for this dimer), the BSSE still represents from 10 to 20% of its BE [7]. Recently studies have concluded that the BSSE becomes negligible if computations are carried out with basis set containing up to 500 orbitals [8].

At the difference of BEs, computations carried out using medium size basis sets at the MP2 level (such as the 6 – 311+G(2d, 2p) or the aug-cc-p*VXZ*, with $X = D$, Q or T) were shown to provide an accurate enough estimate of the incidence of cooperativity on small HB clusters. In particular, the estimate (from Eq. (1)) of the cooperative contributions remains quite unchanged when considering BEs and two-body ΔE_{ij} contributions BSSE corrected or not (*cf.* Refs. [9–11]). Hence, such MP2 *ab initio* computations can be considered as enough accurate to provide meaningful informations regarding cooperative phenomena in HB systems.

2.2. Water Systems: Cooperative Effects and the HB Donor – Acceptor Pattern

From a MP2 *ab initio* study, Mò *et al.* [12] exhibited that cooperative effects affect the properties of isolated water trimers in a different way, depending on their HB network pattern. If we consider the three trimers presented in Figure 1, cooperative effects were shown to be stabilizing and to represent about 17% of the BE of the cyclic trimer **32**, while they are slightly destabilizing for **31** and **32**. Cooperative effects have strong incidence on the geometrical and vibrational properties of **32**. As compared to the water dimer, its interoxygen R(O—O) distances are contracted (up to 0.08 Å) and its OH stretch ν_{OH} frequencies (corresponding to OH groups involved

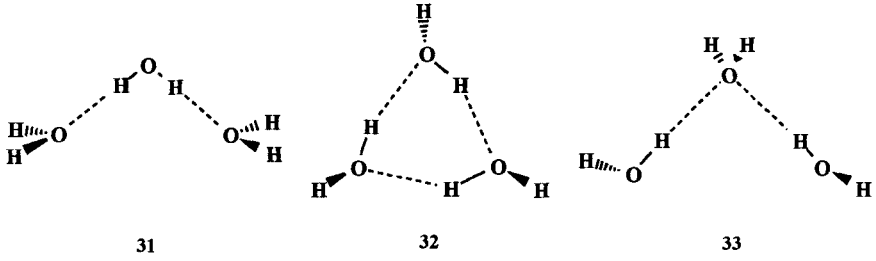

31 32 33

FIGURE 1 Definitions of trimers **31**, **32** and **33**.

in HBs) are redshifted up to 120 cm^{-1}. For **31** and **33**, the trends of both parameters are clearly different: R(O—O)s are increased (up to 0.1 Å) and ν_{OH} values are very close to those observed in the water dimer (*cf.* Tabs. I and II).

TABLE I Geometrical and energetic results for trimers **31**, **32** and **33** and tetramers **40**, **41**, **42** and **43**, estimated from *ab initio* calculations at the MP2/6 – 311 + G(2d, 2p) level, on geometries optimized at the MP2/6–31 + G(d,p) level. Two-body (ΔE_2) and cooperative (greater than the second order, $\Delta E_{N>2}$) contributions in the binding energy (BE) are given in kcal mol^{-1}. Interoxygen R(O—O) distances are given in Å. Definition of HBs I, II, III or IV for **41** and **43** are given in Figure 2

Clusters	*HB*	*R(O—O)*	*BE*	ΔE_2	$\Delta E_{N>2}$
$(H_2O)_2$		2.91	– 5.4		
31		2.95	– 9.7		–
32		2.83	– 16.7	– 13.8	– 2.9
33		3.01	– 7.8		–
40		2.76	– 29.0	– 19.6	– 9.2
41	I	2.83	– 20.0	– 18.7	– 1.3
	II	2.90			
	III	3.09			
	IV	2.93			
42		3.00	– 17.1	– 17.7	+ 0.6
43	I	2.72	– 23.6	– 21.1	– 2.4
	II	2.87			
	III	2.86			

TABLE II OH stretch vibrational frequencies at the MP2/6 – 31 + G(d, p) level for the isolated water dimer, the trimers **31**, **32** and **33**, and the tetramers **40**, **41**, **42** and **43** (in cm^{-1}). OH stretch frequencies corresponding to hydrogen bonded groups are given below the dashed line. For **41** and **43**, a tentative assignment of the frequency to the acceptor OH groups of a particular hydrogen bond is given (*cf.* Fig. 1). OH stretch vibrational frequencies at the MP2/6 – 31 + G(d,p) for the water monomer: 3865 and 4013 cm^{-1} (mean water OH stretch frequency: 3956 cm^{-1})

$(H_2O)_2$	**31**	**32**	**33**	**40**	**41**	**42**	**43**
4002	4003	3969	3991	3955	3984	3987	3982
3983	4003	3968	3986	3955	3969	3987	3979
3863	3913	3965	3982	3955	3964	3949	3945
				3954	3848	3925	3888
							III
3787	3862	3732	3847	3626	3934	3853	3783
					III		II
	3860	3723	3827	3590	3776	3848	3769
					IV		III
	3787	3671	3822	3590	3772	3816	3767
					II		II
				3508	3705	3811	3490
					I		I

In **32**, the HB network corresponds to a molecular arrangement where each of its molecule is simultaneously a proton donor and a proton acceptor of HB, while different HB networks occur in **31** and **33**. In an *ab initio* study at the MP2/aug-cc-pVDZ level, Xantheas and Dunning [9–13] showed that cooperative effects also strongly affect the properties of small cyclic water clusters (from 3 to 6 molecules) where their HB networks correspond to a donor–acceptor pattern: they are stabilizing (and represent up to 25% of the cluster BEs), they are responsible for strong R(O—O) contractions (up to 0.2 Å) and for strong ν_{OH} redshifts (which can reach 400 cm^{-1} in the case of the cyclic water tetramer [13]).

In order to better characterize the relationship between the HB network structure and the incidence of cooperative effects on HB clusters, we have investigated the properties of four water tetramers (**40**, **41**, **42** and **43**, *cf.* Fig. 2) corresponding to various molecular arrangements, using MP2 *ab initio* computations with extended basis sets [10]. In **40** and **43**, all of the molecules adopt a donor–acceptor pattern (in **43**, two molecules are respectively double acceptor and double donor of HBs). Only two molecules

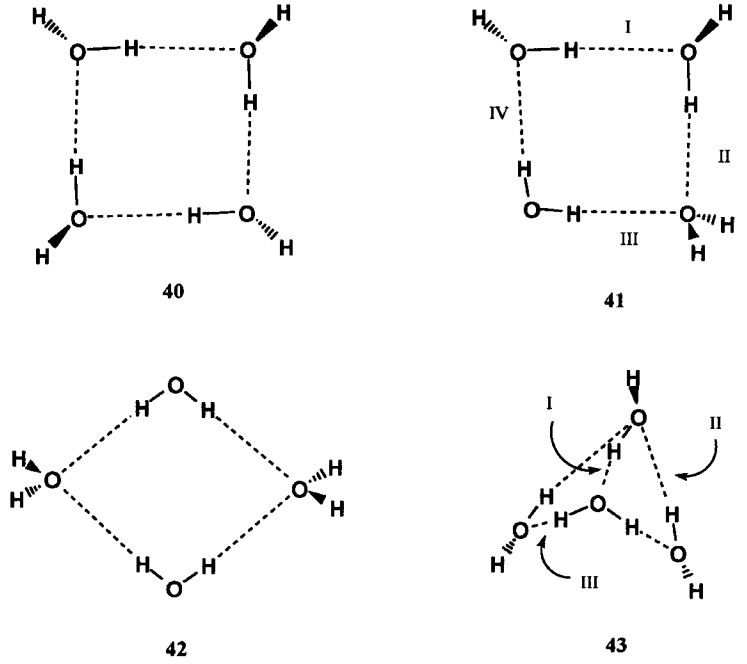

40 **41**

42 **43**

FIGURE 2 Definitions of tetramers **40**, **41**, **42** and **43**, and of hydrogen bonds I, II, III and IV of **41** and I, II and III of **43**.

adopt such a pattern in **41** and no molecule is simultaneously donor and acceptor of HBs in **42**. Tetramer BEs and their decomposition in two-body and cooperative contributions are listed in Table I, as well as their R(O—O) distances. Tetramers ν_{OH} frequencies are summarized in Table II.

The energy ordering predicted by our *ab initio* computations is **40** > **43** > **41** > **42**. Table I shows the cooperative effects to be the essential factor responsible for this energy ordering. In tetramer **40**, cooperative effects give rise to a remarkably high stabilizing contribution (about 9 kcal mol^{-1}), constituting the principal factor responsible for its preferential stabilization. These effects are also stabilizing in tetramers **41** and **43**, but to a lesser extent than for **40**. For **42**, these effects are slightly destabilizing (by about 1 kcal mol^{-1}).

Comparing the structures of tetramers **40**, **41** and **42**, we observe the shortest R(O—O)s to occur in **40** and the longest in **42**. As compared to the water dimer, these distances are shorter in **40** by about 0.15 Å, while for **42**, they are greater by about 0.10 Å. For **41**, R(O—O)s corresponding to the HBs with a local donor–acceptor pattern (*i.e.*, HBs I and II, *cf.* Fig. 2), are more contracted than for the two others (HBs III and IV, *cf.* Tab. I).

In Figure 3, the cooperative contributions in tetramer BE, the mean R(O—O) distances, and the mean ν_{OH} redshifts corresponding to hydrogen

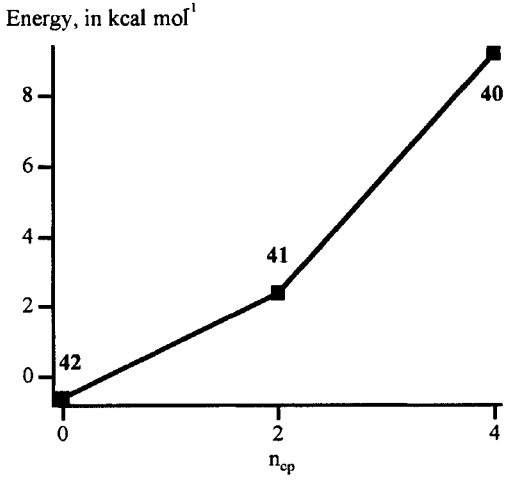

FIGURE 3 (a–c) Cooperative effect consequences in water tetramers **40**, **41** and **42**. For all Figures 2, n_{cp} is the number of hydrogen bonds corresponding to a cyclic pattern (*cf.* text): (a) Stabilizing many-body contribution energies in tetramer binding energy; (b) Mean interoxygen R(O—O) distances; (c) Mean redshifts in the OH stretch frequencies (relative to the mean OH stretch vibrational frequencies of the isolated water monomer) corresponding to hydrogen bonded OH groups.

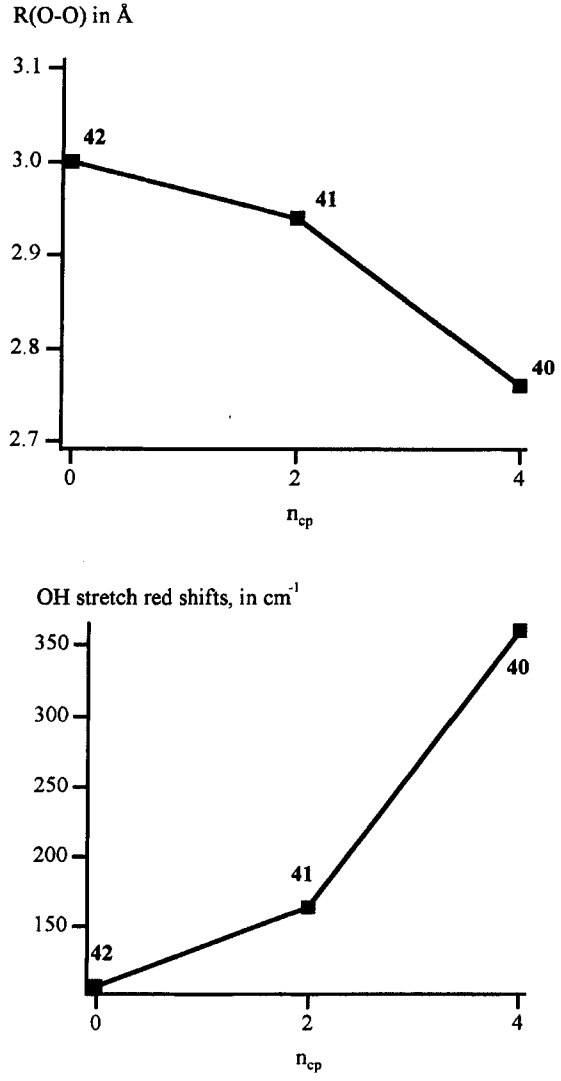

FIGURE 3 (Continued).

bonded OH groups, have been plotted *versus* the number n_{cp} of water molecules adopting a donor–acceptor pattern (*i.e.*, $n_{cp}=4$ for **40**, 2 for **41** and 0 for **42**). The trends observed in Figure 3 for the latter parameters clearly suggest that the weight of cooperative contributions in those three tetramers is related to the number of water molecules adopting a donor–acceptor pattern. Hence, it appears that the more a tetramer has molecules

with a donor–acceptor pattern, the more its HBs are reinforced by cooperativity.

At the difference of tetramers **40**, **41** and **42**, one molecule of **43** is a double proton donor in two HBs (and a proton acceptor in the **43** HB I, *cf.* Fig. 2). From the results summarized in Table I, **43** is by 3.6 kcal mol^{-1} more stable than **41**. Its cooperative contribution is by 1 kcal mol^{-1} greater than that of **41**, but significantly smaller than that of **40** (*cf.* Tab. I). Among the three different types of HB which can be defined for **43** (denoted as HBs I, II and III in Fig. 2), the shortest R(O—O) corresponds to its HB I (namely 2.72 Å). This distance is even shorter than those found in **40** (2.76 Å). We may also observe that the ν_{OH} redshift corresponding to the OH group involved in the **43** HB I is larger than the greatest ν_{OH} redshift observed in **40**, namely 449 and 431 cm^{-1} (*cf.* Tab. II). The corresponding properties (R(O—O)s and ν_{OH} redshifts) of the **43** HBs II and III (with the same HB pattern as in the cyclic trimer **32**) are intermediate between those of **41** and for **42** and are very close to those of the trimer **32** (*cf.* Tabs. I and II).

From the properties of the **43** HBs (and, in particular, those of its HB I), it appears thus that the more a water molecule is a proton donor in different HBs, the more the HBs where it is a proton acceptor are reinforced. The latter cooperative property suggests that water molecules in finite or in bulk-like systems can be classified in three groups with distinct geometrical and vibrational properties, depending on the number n_{HB} of HBs where their hydrogens are involved (in this paper, the following notation is used: molecules with $n_{HB}=0$ are called to be in the state PHB^0, in state PHB^1 for $n_{HB}=1$ and in state PHB^2 for $n_{HB}=2$). Because of the cooperative property described above, molecules in PHB^2 states are expected to be more strongly hydrogen bonded to their neighbors than molecules in PHB^1 and PHB^0 states. Hence, it is then expected that the energetic, geometrical and vibrational properties of water clusters and of bulk-water could primarily result from the number of molecules in each PHB^m state. This hypothesis will be discussed in Section 3.

2.3. Other Types of Hydrogen Bonded Systems

As discussed above in the case of water systems, the cooperative effect incidence on HB systems can be qualitatively predicted just by analyzing the structure of their HB network. In the case of alcoholic systems, Mò *et al.* [14], by investigating three methanol trimers (whose symmetries are similar to those of the water trimers **31**, **32** and **33**) using MP2 *ab initio*

computations, showed that the same trend as in water systems is observed for cooperative effects in alcoholic systems (*i.e.*, the greatest incidence of cooperativity is observed in the cyclic methanol trimer). Szczesniak *et al.* [15], by investigating the properties of three ammonia trimer isomers (one presenting a cyclic donor–acceptor pattern and two an open chain one, similar to the water trimer **31** and **33**) using *ab initio* computations, also showed that the most stable trimer corresponds to the cyclic and that results from stabilizing cooperative effects, whose contributions represent about 10% of its BE. Hence, regardless of the chemical natures of the trimer monomer subunits, it appears that strong stabilizing cooperative effects are only observed in hydrogen bonded trimers with cyclic donor–acceptor pattern.

To evaluate if the above property is also observed in other types of hydrogen bonded trimers, we have investigated (using MP2 *ab initio* computations) five trimers drawn from ammonia (**N**), water (**W**) and formaldehyde (**F**) monomers (*cf.* Fig. 4) [11]: the NH_3 homo trimer N_3, the $[(NH_3)_2, H_2O]$ (WN_2) and the $[NH_3, (H_2O)_2]$ (W_2N) hetero trimers, and two possible $[H_2CO, (H_2O)_2]$ and $[H_2CO, NH_3, H_2O]$ hetero trimer isomers (W_2F and **WNF**). From the energetic results summarized in Table III, it appears that cooperative effects are stabilizing for all of the five trimers

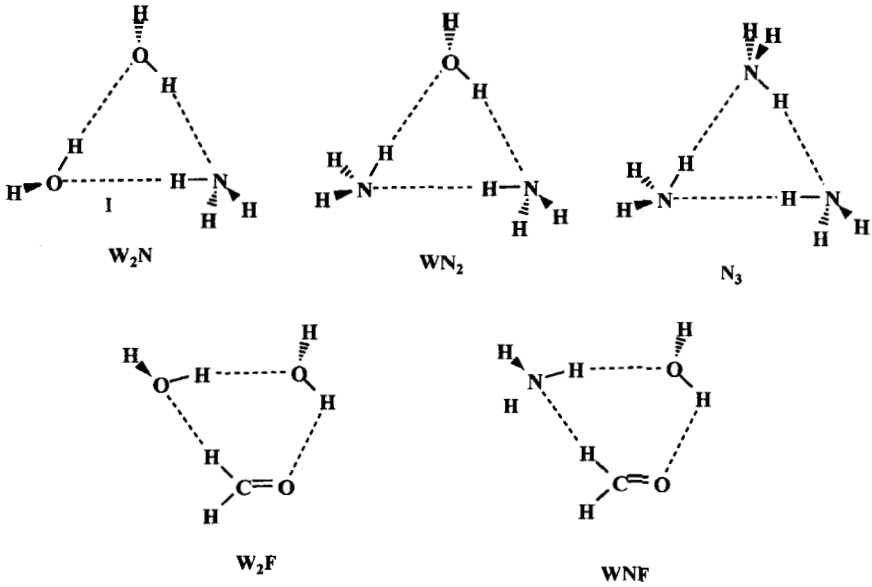

FIGURE 4 Definitions of hetero trimers W_2N, WN_2, N_3, W_2F and WNF.

TABLE III Two-body and three-body contributions in trimer binding energies. E_{relax} corresponds to the intramolecular relaxation energy of each trimer; ΔE_2: total two-body energy; BE: total binding energy of each trimer; ΔE_3: total three-body contributions in trimer BE; %coop: percentage of three-body contributions in trimer BE. All energetical results in kcal mol^{-1}

	W_3	W_2N	WN_2	N_3	W_2F	WNF
BE	16.40	16.4	14.3	10.9	14.5	12.0
ΔE_2	13.54	14.20	12.61	9.88	12.70	10.62
ΔE_3	2.86	2.23	2.03	1.01	1.78	1.35
E_{relax}	0.72	0.29	0.20	0.01	0.14	0.11
%coop	17.5	13.6	14.2	9.2	12.3	11.3

and that they represent from 10 to 17% of their BEs. However, the cooperative contributions for trimers where several non-typical X-H—Y HBs occurs (such as C-H—Y, N-H—N [16] and N-H—O [16] HBs, occurring in the N_3, W_2F and **WNF** trimers) are smaller than those observed in the cyclic water trimer **32** (where three typical O-H—O HBs occur), by about 35%. For W_2N and WN_2, the cooperative contributions are also smaller than for **32**, but to a lesser extent than for N_3, W_2F and **WNF**. Apparently, the less a trimer contains typical HBs, the less it is stabilized by cooperativity.

Cooperative effects have also strong consequences on the geometrical and vibrational properties of the X-H—Y HBs of the five trimers considered. From the results presented in Ref. [11], the cooperative effect incidence on the geometrical and vibrational properties of typical HBs (*i.e.*, for (X, Y) = (O, O) or (O, N)) were shown to be very close, regardless of the trimer type: R(X—Y) distances are contracted and ν_{XH} frequencies are redshifted as compared to their values in isolated dimers. The mean values corresponding to the R(X—Y) contractions (δR(X—Y)) and to the of ν_{XH} redshifts ($\delta\nu_{XH}$) for a particular type of X-H—Y HB (estimated from their values in all of the trimers where the HB occurs) are summarized in Table IV for the above typical HBs. As observed in this table, the consequences of cooperativity on a particular type of HB seems to primarily depend on the chemical nature of that HB. For instance, the mean parameter values corresponding to N-H—O HBs (as defined in the isolated **WN** dimer) observed in the W_2N and WN_2 trimers are: $\langle\delta R(\text{N—O})\rangle = 0.11 \pm 0.02$ Å and $\langle\delta\nu_{OH}\rangle = 136 \pm 28\,\text{cm}^{-1}$. For O-H—O(sp^3) HBs (as defined in the water dimer), the reinforcements of their properties observed in W_2N, W_2F and **32** are also very close: $\langle\delta R(\text{O—O})\rangle = 0.11 \pm 0.01$ Å and $\langle\delta\nu_{OH}\rangle = 113 \pm 13\,\text{cm}^{-1}$ (*cf.* Tab. IV). Interestingly, it is worth noticing

that the magnitude of the variation of the above parameter correlates with the ordering in the BEs obtained for the dimers where those HBs occur (*i.e.*, O-H—N(sp^3) > O-H—O(sp^3 or sp^3) > N-H—O(sp^3 or sp^3) > N-H—N(sp^3), *cf.* Fig. 5 and Ref. [11]).

TABLE IV Mean values of δR(X—Y) (Å) and $\delta\nu_{XH}$(cm^{-1}) parameters, for "typical" hydrogen bonds (*cf.* text). HB type: dimer where the X-H—Y interaction occurs (*cf.* Fig. 5 and Ref. [11])

HB type	$\langle\delta R(X—Y)\rangle$	$\langle\delta\nu_{XH}\rangle$
W_2	0.10 ± 0.01	113 ± 13
WN	0.11 ± 0.02	136 ± 28
WF	0.03	87
N_2	0.09 ± 0.03	50 ± 2
NW	0.17 ± 0.01	20 ± 3

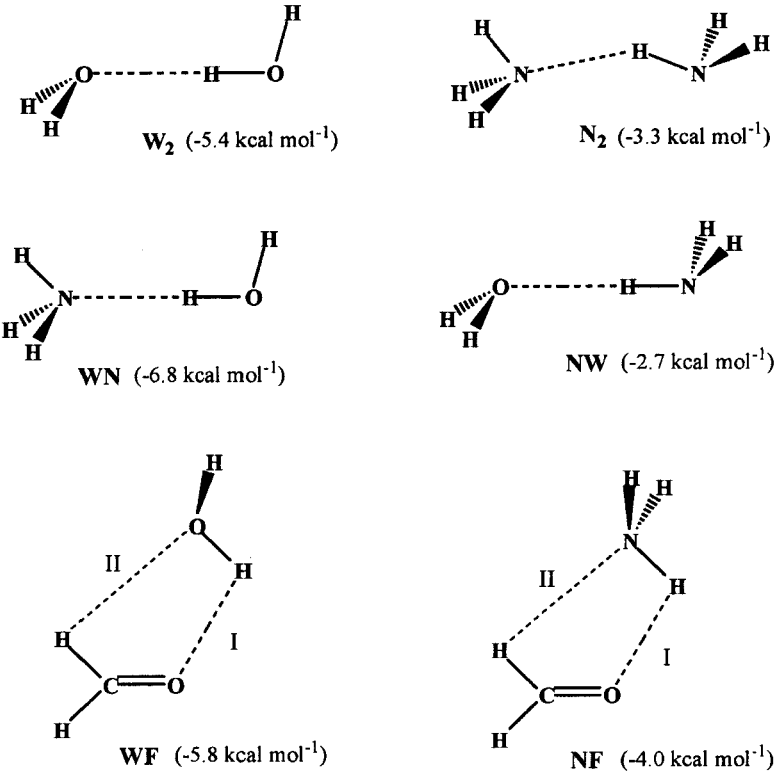

FIGURE 5 Dimer definitions (their binding energies as obtained from MP2/6 − 311 + G(2df, 2p) computations are given in parentheses).

In Table IV, the R(C-Y) distances and the ν_{CH} frequencies corresponding to the non-typical C-H—O(sp^3), and C-H—N(sp^3) HBs are not reported. However, they were shown to be unaffected or to follow an opposite trend from dimers to trimers. For instance, as compared to their values in **WF** and **NF** dimers, the R(C-Y) distances are increased by about 0.16 Å in both the $\mathbf{W_2F}$ and **WNF** trimers; two of the **WNF** and $\mathbf{W_2F}$ ν_{CH}s are smoothly blueshifted (from 6 to 23 cm^{-1}), one unchanged and one redshifted (however, only by 6 cm^{-1}). Hence, the trends from dimers to trimers for several properties of C-H—Y interactions are clearly different from those observed in the case of typical HBs.

2.4. Origin of Cooperative Effects in Hydrogen Bonded Systems

The origin of such effects in weakly hydrogen bonded systems (in particular, in water clusters) is still far from being well understood. In the particular case of water, cooperative polarization effects have been shown to represent a sizeable part of these effects [17], and the explicit introduction of a many-body polarization energy term was shown to provide a major improvement in the quality of molecular simulations of liquid water [18]. Recent simulations on water aggregates using polarizable mechanics procedures such as ASP-W_n [19] and SIBFA [20] also showed this term to be essential to account for the cooperative nature of such aggregates, as well as their anti-cooperative one in some cases.

However, a X-H—Y HB may be also considered as the result of a charge transfer from the lone pairs of the proton acceptor Y (taken as an sp^3 orbital, l_d) towards the antibond σ^* orbital of the proton donor XH (and was maybe proposed for the first time by C. A. Coulson in 1957 [21]). In the particular case of water, this approach has been recently confirmed by an X-ray diffraction experiment [22] regarding ice, which concluded that the HB among water molecules is in part covalent. This HB approach could explain the cooperative effect incidence on cyclic donor–acceptor HB patterns. The charge transfer from a proton acceptor to a donor will slightly destabilize the lone pairs of the proton donor. If this donor is also acceptor in another HB, this destabilization will reinforce the interaction between one of its lone pair and an antibonding orbital OH of the new proton donor, and, as a consequence, the new HB. As all of the molecules involved in donor–acceptor patterns simultaneously act as donor and acceptor, this suggest that a part of the cooperative effects related to those patterns arises from the previous phenomena. Such cooperative topological

effects are expected to have no influence for other type of HB pattern (such as those observed in trimers **31** and **33**), because no molecule in either trimers is simultaneously donor and acceptor. However, as the amount of charge transferred does not represent an observable, it is difficult to quantify the influence of the cooperative charge transfer effects in weakly hydrogen bonded systems in energetic terms. In a previous study [10], where the possible incidence of charge transfer phenomena were compared to those of polarization effects in the case of the four water tetramers described in Figure 2, we have shown that both the latter possible cooperative effects have the same trends in those tetramers (*i.e.*, when polarization effects lead to strong stabilizing cooperative effects then charge transfer effects should also lead to similar òstabilizing effects, and *vice-versa*).

As a conclusion, regardless of their origin in terms of charge transfer phenomena or polarization effects, cooperative effects appear thus to be of importance to understand the energetic, vibrational and geometrical properties of systems where HBs occur. In particular, those effects could be fundamental to understand the solvation processes in aqueous or alcoholic solutions of biochemical systems (su as proteins and carbohydrates) and also to understand the physical phenomena occurring at the interface of solid/liquid and liquid/vapor systems involving water molecules. However, accurate *ab initio* computations for such sizeable molecular systems are still far beyond from the current computational resources, and, therefore, the study of those systems can be made only by considering empirical or *ab initio* derived models. However, the results presented in that section clearly exhibit the necessity for such models to reproduce the great incidence of cooperativity in systems presenting donor–acceptor HB patterns. Recently, we have proposed one such model, called TCPE for topological and classical polarization effects [23], which is presented in Section 3.

3. THE TCPE MODEL FOR HYDROGEN BONDED SYSTEMS

3.1. Analytical Expression

The potential energy function is taken as follows:

$$\Delta E = E_{\text{rep}} + E_{\text{qq}} + E_{\text{rel}} + E_{\text{pol}} + E_{\text{HB}} \tag{2}$$

E_{rep}, E_{qq} and E_{rel} correspond to a repulsive, a charge–charge electrostatic and an intramolecular relaxation terms (atomic charges for E_{qq} were

assigned to reproduce the gas phase water dipole moment, and for the analytical expression of the E_{rel}, *cf.* Ref. [24]). E_{pol} stands for a molecular many-body polarization term:

$$E_{pol} = -\frac{1}{2}\sum_i \vec{\mu}_i \cdot \vec{E}_i^0 \tag{3}$$

The sum runs over all molecules, $\vec{E}_i^0$ is the electric field created by the charges defined for E_{qq} and $\vec{\mu}_i$ the molecular induced dipole moment:

$$\vec{\mu}_i = \alpha\left(\vec{E}_i^0 + \frac{1}{4\pi\varepsilon_0}\sum_{j\neq i} T_{ij}\vec{\mu}_j\right) \tag{4}$$

T_{ij} is the polarizability tensor and α the water molecular polarizability. Equation (4) is solved using a classical iterative scheme, with iterations continuing until the root mean square of the difference in the induced dipole between successive iterations is less than 10^{-5} Debye per molecule. The E_{HB} term stands for an anisotropic function:

$$E_{HB} = \sum f(r)g(\theta)p(\psi) \tag{5}$$

$$\begin{aligned} f(r) &= D_c \exp\left(-\frac{(r-r_c)^2}{\gamma_r}\right) \\ g(\theta) &= \exp\left(-\frac{(\theta-\theta_c)^2}{\gamma_\theta}\right) + \exp\left(-\frac{(\theta+\theta_c)^2}{\gamma_\theta}\right) \\ p(\psi) &= \exp\left(-\frac{(\psi-\psi_c)^2}{\gamma_\theta}\right) \end{aligned} \tag{6}$$

The geometrical parameters r, θ and ψ are defined in Figure 5 (the remaining parameters were given in a previous paper [23]). The influence of cooperative effects on donor–acceptor patterns has been accounted for in TCPE by altering the D_e and r_e parameters. For a molecule acting as a proton acceptor, they are not constant but they linearly depend on the E_{HB} value when the molecule acts as a proton donor in one or two HBs:

$$\begin{aligned} D_c(R,\Psi) &= d_c\left(1 + \xi_1 \sum F(R)G(\Psi)\right) \\ r_c(R,\Psi) &= r_c\left(1 - \xi_2 \sum F(R)G(\Psi)\right) \end{aligned} \tag{7}$$

F, G, R and Ψ have the same definition as the f and g functions, and the r and ψ variables (*cf.* Eq. (6) and Fig. 6). d_e and r_e parameters of F and G are constant. All parameters were assigned to reproduce MP2 *ab initio* results on the water dimer and cyclic trimer [23].

3.2. Accuracy of the TCPE Model

As compared to high level *ab initio* computations, the TPCE model was shown to reproduce most of their predictions on small water clusters from two to eight molecules. For instance, as predicted by MP2 *ab initio* computations [25], TCPE predicts the five water hexamers, corresponding to arrangements called Cage, Prism, Book, Boat and Chair (*cf.* [2f]), to be isoenergetic within 1 kcal mol^{-1} (with BEs of about 48 kcal mol^{-1} [23]). In the case of water tetramers, TCPE is also able to reproduce the specific incidence of cooperativity on the four tetramers **40**, **41**, **42** and **43** described in Section 2.2, with results differing from *ab initio* ones at most by 1.5 kcal mol^{-1} [26]. All of these results therefore exhibit the good accuracy of the TCPE model in describing cooperative effects in water systems. It has also appeared that the TCPE model provides one of the most accurate description of the water dimer potential energy surface as described by high level *ab initio* computations [7], and it has been able to predict the existence of particular splittings in the water dimer energy levels (resulting from tunneling motions [2a]), which no other model do [27]. The TCPE model appears also to be readily transferable to other types of HB, just by adapting some of its parameters (*cf.* Ref. [28] for the particular case of alcohols).

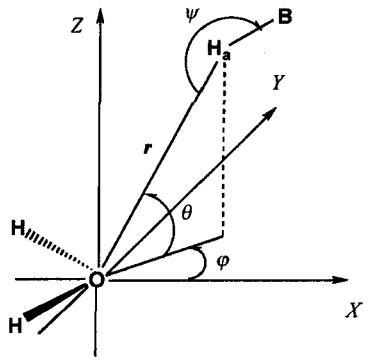

FIGURE 6 Definitions of the r, θ and ψ variables of the E_{HB} term. The X and Y axes are in the molecular plane, the Z axis is orthogonal to this plane.

As discussed in Section 2.2, the properties of water clusters and of bulk water could be interpreted as resulting from the properties of the HB networks occurring in them in terms of PHB^m states (*cf.* Section 2.2). The originality of the TCPE model arises from the presence of the specific many-body HB energy term described in Eqs. (5), (6) and (7), which has been introduced to reproduce the remarkable incidence of cooperative effects on the HBs resulting from molecules in those state. As the estimate of this many-body term needs the knowledge of the molecular structure around each water molecule, it can also be used to define a new local structural index. In particular, as it will be described below, it is very easy to determine the respective weight of molecules in each PHB^m state in the cluster using this local index. The purpose of Section 4 is to evaluate this hypothesis by studying the thermal molecular rearrangements in a $(H_2O)_{24}$ cluster, using classical molecular dynamics (MD) techniques and the TCPE model.

4. STUDY OF THE HB NETWORK FLUCTUATION IN A $(H_2O)_{24}$ CLUSTER

4.1. Molecular Dynamic Details

The starting $(H_2O)_{24}$ structure for the MD runs corresponds to the most stable minimum obtained by systematic quenching from a high energy MD trajectory. The MD configurations were energy-optimized using a Conjugate-Gradient algorithm. The most stable quenched configurations were then gradient-optimized and the second derivatives performed to control the nature of these stationary points. The most stable structure so obtained (corresponding to a minimum) is given in Figure 7. Its BE is of $-285.1\,\text{kcal mol}^{-1}$. By comparing this value to that obtained with the pairwise PW model [23] (derived from TCPE), cooperative effects appear to be stabilizing for this cluster and to represent about 30% of its BE.

The propagator chosen was a two-stage canonical RKN method of second order [29] with an integration time step of 0.4 fs. The simulations were performed from 600 ps to 1 ns (including an equilibration step of 200 ps, the longest trajectories correspond to a system around the melting point or in the liquid-like state). No cutoff was imposed to the electrical and the polarization term of TCPE. Translation of and rotation about the cluster center of mass were both eliminated at the start of each MD run. Configurations were sampled at every 10 fs to compute the statistical data, after having discarded the configurations of the equilibration step

(the first 200 ps). Hence, from 40000 to 80 000 different configurations were considered during the trajectory analyses. From the starting $(H_2O)_{24}$ structure described above, twelve MD runs, corresponding to total energies regularly spaced by the equivalent of 25 K, were performed in the (E, N) ensemble.

4.2. Definition a New Structural Local Index

As observed in Eq. (6), the $D_e(R, \Psi)$ function of the E_{HB} term for a given water molecule depends on the number of HBs where its protons are involved. If none of its protons is involved in a HB, then $D_e(R, \Psi)$ is equal to d_e, to $d_e(1+\xi)$ when only one of its protons is involved in a HB and to $d_e(1+2\xi)$ when its two protons are involved in two HBs. Obviously, during a MD run, the exact value of the $D_e(R, \Psi)$ function for each molecule is expected to fluctuate around the latter ideal values.

To evaluate the number of molecules in PHB^m states during a simulation, the $\delta_{HB}(t)$ function corresponding to the distribution function of the $D_e(R, \Psi)$ term at time t has been introduced. A summation of $\delta_{HB}(t)$ functions (obtained after a simulation time length of 10 ps, representing 1000 configurations) is reported in Figure 8 (it was obtained from a MD run of the $(H_2O)_{24}$ cluster corresponding to a total energy of $-7.0\,\text{kcal mol}^{-1}$ per molecule, the system is then in a liquid-like state). As observed, the peaks corresponding to the PHB^1 and PHB^2 state are well defined (and centered at the above ideal values), while no peak corresponding to molecules in PHB^0 state is observed. The proportions of molecules in the PHB^m states

FIGURE 7 Starting $(H_2O)_{24}$ structure for the MD runs as obtained after systematic quenching of a high energy trajectory of 1 ns.

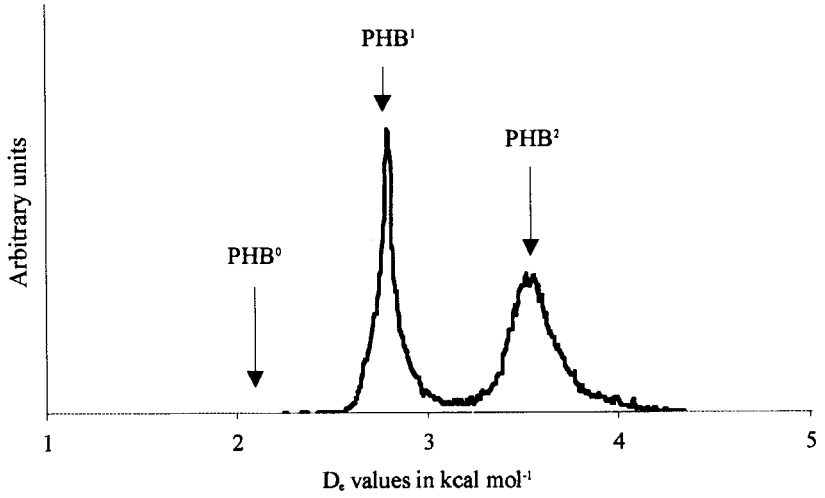

FIGURE 8 Distribution function of the $D_e(R,\Psi)$ term (summed over a simulation time length of 10 ps) as obtained from a MD run of the $(H_2O)_{24}$ cluster at the total energy of -7.0 kcal mol^{-1} K^{-1} per molecule. The ideal D_e value for a molecule in a particular PHB^m state are shown by an arrow.

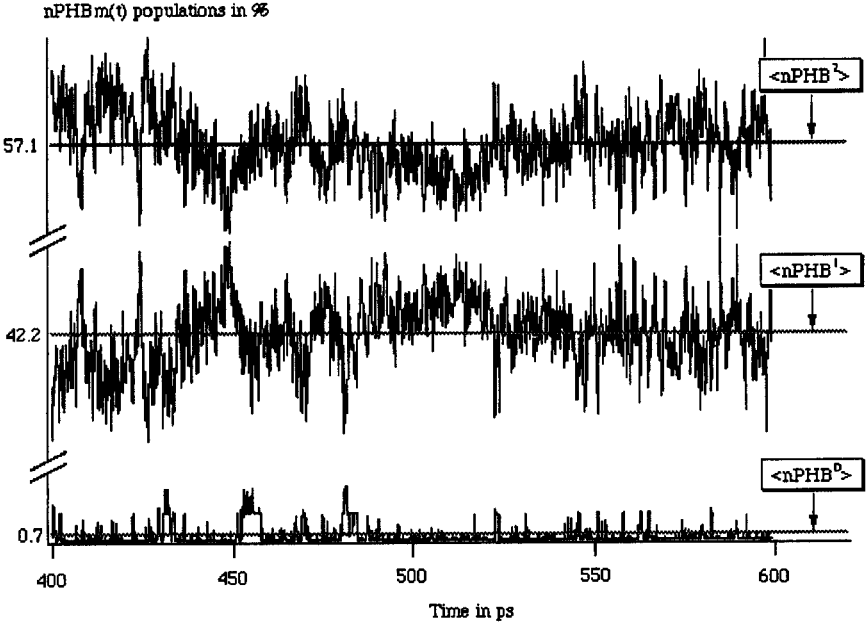

FIGURE 9 Fluctuations in the proportions of molecules in each PHB_m state around their mean $\langle nPHB_m \rangle$ values along a trajectory of 0.2 ns (after 0.4 ns of equilibration) with the same characteristics as in Figure 7.

at time t, $nPHB^m(t)$, are readily obtained by integrating the $\delta_{HB}(t)$ function. In Figure 9, $nPHB^m(t)$ functions so obtained are plotted *versus* time. One remarkable feature of Figure 9 is that the $nPHB^m(t)$ functions fluctuate around their mean $\langle nPHB^m \rangle$ values, and the proportion of molecule in the PHB^0 state is negligible. Similar results were obtained for $(H_2O)_8$ and $(H_2O)_{12}$ clusters [30].

This therefore suggests that the dynamical molecular rearrangements among the PHB^m molecules in the $(H_2O)_{24}$ cluster are highly correlated, so that the $\langle nPHB^m \rangle$ values are constant for trajectories corresponding to a given total energy. Hence, $\langle nPHB^m \rangle$ values are characteristic of a MD run, indicating that the δ_{HB} local index is very useful to describe a water cluster structure in terms of PHB^m state. However, due to the small size of the cluster considered in the present study, the fluctuation in the $\langle nPHB^m \rangle$ values are expected not to be negligible and they were computed as follows:

$$\Delta x = \sqrt{\sum (x - \bar{x})^2}$$

x corresponds to the proportion $nPHB^m$ of water molecules in the PHB^m state at time t, $\bar{x}$ to averaged values, and the sum runs over all the simulation time length. For the $(H_2O)_{24}$ cluster, the Δx are of 6.5% for the PHB^1 and PHB^2 sta. However, from a comparisons of the fluctuations obtained in the case of the $(H_2O)_8$ and $(H_2O)_{12}$ clusters [30], it appears that the Δx fluctuations are of the form $1/\sqrt{N}$, with N the molecular size of the cluster.

4.3. Dynamical Results

To characterize the physical state of the $(H_{2O)_{24}}$ cluster in terms of solid-like and liquid-like state, the Lindemann's index, defined as follows, has been used:

$$\delta_R = \frac{2}{N(N-1)} \sum_{i<j} \left(\overline{R_{ij}^2} - \overline{R_{ij}}^2 \right)^{1/2} \tag{8}$$

R_{ij} represent the distance between the centers of mass of the ith and jth molecules. Usually, the system is considered to be in a liquid-like state when $\delta_R > 0.1$ (and in the solid-like state when $\delta_R < 0.1$). The Lindemann's index and the mean temperature (as classically defined from the kinetic energy) are plotted in Figure 10 as a function of the total energy. The proportions $\langle nPHB^m \rangle$ of molecules in each PHB^m state are plotted *versus* the total energy in Figure 11.

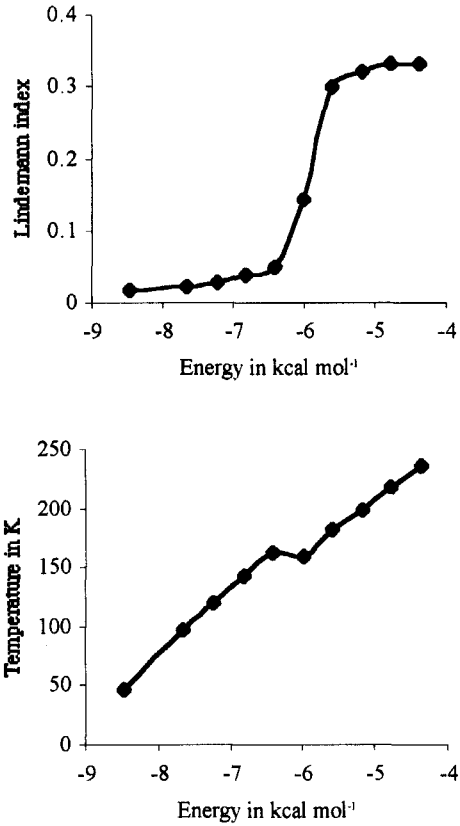

FIGURE 10 MD run averages for the $(H_2O)_{24}$ cluster: Lindemann criterion (Top) and caloric curve (bottom).

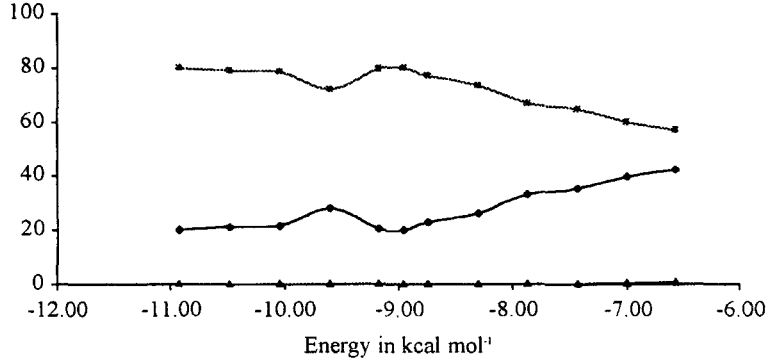

FIGURE 11 MD run averages for the $(H_2O)_{24}$ cluster: PHB^m populations in percent. Squares correspond to $\langle nPHB^2 \rangle$, lozenges to $\langle nPHB^1 \rangle$ and triangles to $\langle nPHB^0 \rangle$.

The proportions of molecules in the PHB^0 state is almost negligible as compared to molecules in PHB^1 and PHB^2 states, they represent at most about 1.7% for MD runs corresponding to the highest total energies. For molecules in the PHB^1 and PHB^2 states, three domains with different trends for $\langle nPHB^m \rangle$ values are clearly observed in Figure 10:

1. At the lowest total energies, the proportions of molecules in each PHB^m state is almost constant, reflecting the solid-like behavior of the cluster in this range of energies ($\delta_R < 0.1$). In that domain of energy, the $\langle nPHB^m \rangle$ fluctuations are small and represent less than 2%.
2. At the highest total energies, the $\langle nPHB^m \rangle$ values corresponding to the PHB^1 and PHB^2 states are linear functions (opposite in trends) of the total energy: the $\langle nPHB^m \rangle$ are growing functions for PHB^1 molecules and decreasing ones for PHB^2. This domain is also characterized by a δ_R index greater than 0.2, indicating that the cluster can be considered to be in a liquid-like state in this energy domain. The trends of the $\langle nPHB^m \rangle$ values in this energy domain exhibits the progressive disorganization of the cluster structure, from highly organized ones (with an important proportion of molecules in the PHB^2 state) towards disorganized ones (with an increasing number of molecules in the PHB^1 state). Not surprisingly, the $\langle nPHB^m \rangle$ fluctuations are much more important than in the solid-like energy region. They are from twice to four times greater, however, they were shown to decrease with the cluster size (*cf.* Section 4.2).
3. Lastly, in the finite range of energy located between the above domains and around the melting point, the $\langle nPHB^m \rangle$ trends for the three clusters are characterized by abrupt changes from their values in the solid-like region towards their values in the liquid-like region, as do the Lindemann's index δ_R. The analysis of short time averaged temperatures (STAT) performed in this domain of energy show a multimodal distribution of the STAT for the $(H_2O)_{24}$ cluster. Such multimodal distributions of the STAT in a finite range of energy were previously evidenced by Wales and Ohmine [31] in the case of small $(H_2O)_8$ and $(H_2O)_{12}$ clusters (theoretically investigated using a pairwise model). The existence of such STAT distribution is usually interpreted as resulting from the existence of a dynamical coexistence between solid-like and liquid-like forms. According to this hypothesis, the unusual trends of $\langle nPHB^m \rangle$ in this finite range of energy (as compared to the trends observed in the solid-like and liquid-like energy domain) can be interpreted as resulting from the coexistence phenomenon.

The oxygen–oxygen gOO distribution functions were also computed using classical formula. Some of those functions are represented in Figure 12 (they are derived from trajectories corresponding to mean temperatures of about 167, 197 and 258 K). In the liquid-like energy domain, the position of the first maximum of those functions increases with temperature from 2.70 Å (lowest energy MD runs) towards 2.74 Å (highest energy MD runs). Those values have to be compared to the position of the first maximum of the gOO function of liquid water at ambient conditions (about 2.80 Å). The shorter distance for the first gOO peaks observed for the $(H_2O)_{24}$ cluster as compared to liquid water can be due to the stronger mean molecular total dipole moment for this cluster (2.9 ± 0.2 Debye for the highest energy trajectory) than for liquid water (2.6 Debye). Stronger molecular dipole moments lead to stronger polarization interactions in the $(H_2O)_{24}$ cluster which can be at the origin of its more compact structure as compared to water.

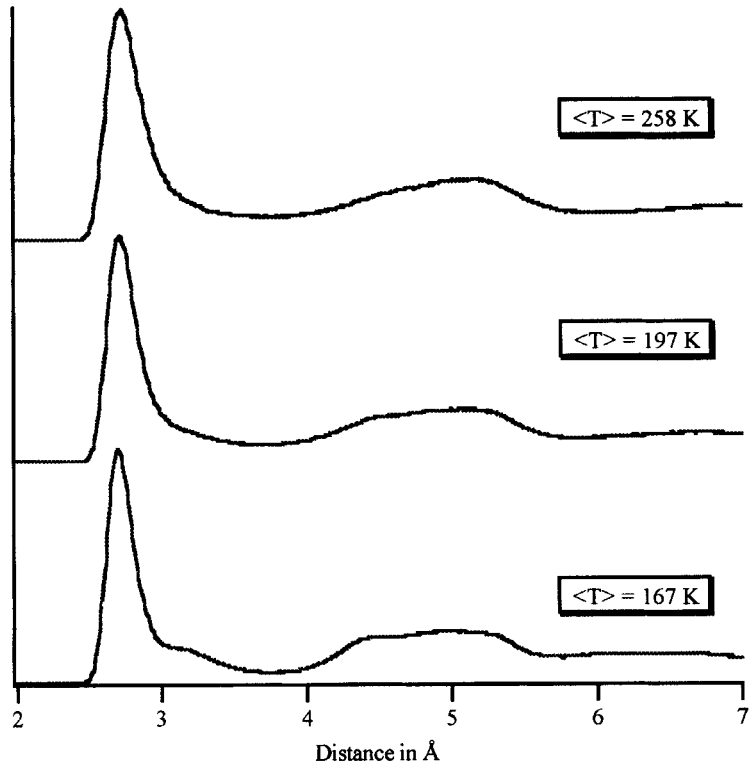

FIGURE 12 Oxygen–oxygen distribution functions as obtained from trajectories corresponding respectively to mean temperatures of 167, 197 and 258 K.

4.4. Thermodynamic Properties of the PHB_2/PHB_1 Equilibrium

From the results regarding the proportions of molecules in each PHB^m state, it appears that the dynamical rearrangement in the $(H_2O)_{24}$ cluster can be interpreted as resulting from a dynamical equilibrium between molecules in PHB^1 and PHB^2 states, because:

1. molecules in the PHB^0 states are negligible in the range of temperatures here considered.
2. the proportions of molecules in the PHB^1 and PHB^2 states are constant for each trajectory. (even if the fluctuations in the mean $\langle nPHB^m \rangle$ proportion values in the liquid-like domain are strong, they were shown to decrease with the cluster molecular size).

In order to evaluate the properties of the PHB^2/PHB^1 equilibrium, the parameter K_{24} has been defined as follows:

$$K_{24} = \frac{\langle nPHB^2 \rangle}{\langle nPHB^1 \rangle} \tag{10}$$

In Figure 13, the $R_a \ln(K_{24})$ function (with $R_a = 0.0199\,\text{kcal mol}^{-1}$) is plotted *versus* the inverse of the mean temperature for MD runs where the cluster is in a liquid-state. From this Van't Hoff plot, it appears that a

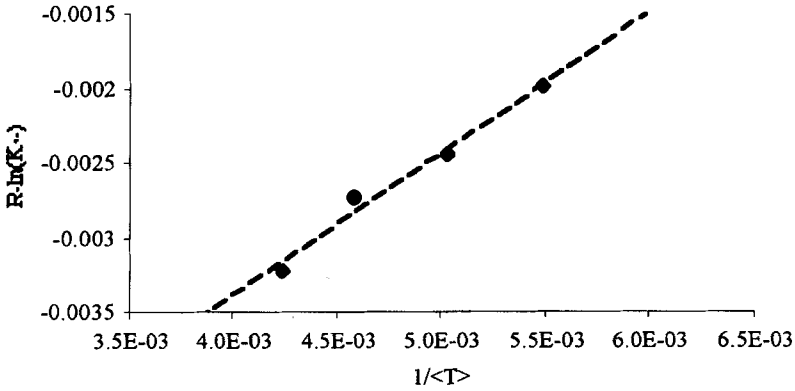

FIGURE 13 Logarithm of the ratio of the evolving concentrations of molecules in the PHB^2 and PHB^1 states, plotted *vs.* the inverse of the $\langle T \rangle$ temperature, from trajectories corresponding to the liquid-like energy domain ($\langle T \rangle$ greater than 160 K). The enthalpy change ΔH (slope) is of 1.1 kcal mol^{-1} and the entropy change ΔS of -4.0 cal mol^{-1} K^{-1}. The correlation factor is of 0.987. The uncertainties have been respectively estimated at 0.2 kcal mol^{-1} (ΔH) and 1 cal mol^{-1} K^{-1} (ΔS, *cf.* Ref. [30]).

linear relation exists between $R_a\ln(K_{24})$ and $1/\langle T\rangle$ (the correlation factor is of 0.99). From the existence of such a linear relationship, the enthalpy (ΔH) and entropy (ΔS) changes corresponding to the PHB^2/PHB^1 equilibrium for the $(H_2O)_{24}$ cluster have been computed to respectively 1.1 ± 0.2 kcal mol^{-1} and -4 ± 1 cal mol^{-1} K^{-1}.

Such an equilibrium between two species of hydrogen bonded molecules could be related to that experimentally observed in the case of liquid water at ambient conditions. From the analysis of Raman and infrared spectra, Walfaren *et al.* [32] and more recently by Libnau *et al.* [33] argued that water molecules arrange themselves in two different classes of hydrogen bonded molecules which are in equilibrium. The experimental enthalpy change corresponding to this equilibrium estimated by the latter authors is respectively of 2.6 (Walfaren) and 2.2 kcal mol^{-1} (Libnau) and the entropy change of -6.2 (Walfaren) and -7.3 cal mol^{-1} K^{-1} (Libnau). Hence, it appears that both the theoretical ΔH and ΔS for the $(H_2O)_{24}$ cluster are of the same order of magnitude than the values experimentally reported for liquid water at ambient conditions, suggesting that the equilibrium observed in the case of liquid water could correspond to a PHB^2/PHB^1 equilibrium.

Hence, the results regarding the small $(H_2O)_{24}$ cluster exhibits that the analysis of water HB networks in terms of PHB^m states represents an encouraging way of characterizing the properties of such systems. Such an approach may also be usefully considered to explain the different properties of supercritical water as compared to liquid water at ambient conditions. In particular, because of the lower molecular density of supercritical water as compared liquid water, the different properties of supercritical water can result from the existence of a PHB^1/PHB^0 equilibrium instead of a PHB^2/PHB^1 one.

5. CONCLUSION

From the results discussed in the present paper, it appears that cooperative effects have a strong incidence on hydrogen bonded systems, in particular, those presenting X-H—Y cyclic patterns, and from the MD simulation study devoted to a small $(H_2O)_{24}$ cluster, it appears that this incidence could be at the origin of the dynamical properties of bulk-water and could also explain the unusual properties of water in supercritical states. Regarding systems of biochemical interest (such as proteins and DNA), cooperative effects could also be of importance to understand their solvation processes

in aqueous solutions as the results presented in a previous paper [34] suggest in the particular case of ethane-1,2 diol.

Acknowledgements

Pr. A. Fuchs and N. Gresh are greatly acknowledged for helpful diussions. Pr. S. Hammerum and Pr. J.-M. Launay are also greatly acknowledged for their help and support. The Laboratoire de physique des lasers, atomes et molecules is "unité associée au CNRS". The "Centre d'Etude et de Recherche Lasers et Applications" (CERLA) is supported by the ministère chargé de la Recherche, the Région Nord-Pas de Calais and the Fonds Européen de Développement Economique des Régions.

References

[1] Crabtree, R. H. (1998). *Science*, **282**, 2000.
[2] (a) Pugliano, N. and Saykally, R. J. (1992). *Science*, **257**, 1937; (b) Liu, K., Loeser, J. G., Elrod, M. J., Host, B. C., Rzepiela, J. A., Pugliano, N. and Saykally, R. J. (1994). *J. Am. Chem. Soc.*, **116**, 3507; (c) Cruzan, J. D., Braly, L. B., Liu, K., Brown, M. G., Loeser, J. G. and Saykally, R. J. (1996). *Science*, **271**, 59; (d) Liu, K., Brown, G., Cruzan, J. D. and Saykally, R. J. (1996). *Science*, **271**, 62; (e) Liu, K., Cruzan, J. D. and Saykally, R. J., *Science*, **271**, 929; (f) Liu, K., Brown, M. G., Carter, C., Saykally, R. J., Gregory, J. K. and Clary, D. C., *Nature*, **381**, 501; Paul, J. B., Collier, C. P., Saykally, R. J., Scherer, J. J. and OíKeefe, A., *J. Phys. Chem. A*, **101**, 5211.
[3] Gruenloh, C. J., Carney, J. R., Arrington, C. A., Zwier, T. S., Fredericks, S. Y. and Jordan, K. D. (1997). *Science*, **276**, 1678; Pribble, R. N. and Zwier, T. S. (1994). *Science*, **265**, 75; Pribble, R. N. and Zwier, T. S. (1994). *J. Chem. Soc., Faraday Discuss*, **97**, 229.
[4] Huisken, F., Kaloudis, M. and Kulcke, A. (1996). *J. Chem. Phys.*, **104**, 17.
[5] Loeser, J. G., Schmuttenmaer, C. A., Cohen, R. C., Elrod, M. J., Steyert, D. W., Saykally, R. J., Bumgarner, R. E. and Blake, G. A. (1992). *J. Chem. Phys.*, **97**, 4727; Havenith, M., Cohen, R. C., Bursarow, K. L., Gwo, D.-H., Lee, Y. T. and Saykally, R. J. (1991). *J. Chem. Phys.*, **94**, 4776; Havenith, M., Linnartz, H., Zwart, E., Kips, A., ter Meulen, J. J. and Meerts, W. L. (1992). *Chem. Phys. Lett.*, **193**, 261; Linnartz, H., Kips, A., Meerts, W. L. and Havenith, M. (1993). *J. Chem. Phys.*, **99**, 2449.
[6] Lovas, F. J. and Lugez, C. L. (1996). *J. Mol. Spectrosc.*, **179**, 320.
[7] Smith, B. J., Swanton, D. J., Pople, J. A. and Schaefer III, H. F. (1990). *J. Chem. Phys.*, **92**, 1240.
[8] Feyreisen, M. W., Feller, D. and Dixon, D. A. (1996). *J. Phys. Chem.*, **100**, 2993.
[9] Xantheas, S. S. (1994). *J. Chem. Phys.*, **100**, 7523.
[10] Masella, M., Gresh, N. and Flament, J.-P. (1998). *J. Chem. Soc., Faraday Trans.*, **94**, 2745.
[11] Masella, M. and Flament, J.-P. (1999). *J. Chem. Phys.*, **110**, 7245.
[12] Mò, O., Yanez, M. and Elguero, J. (1992). *J. Chem. Phys.*, **97**, 6628.
[13] Xantheas, S. S. and Dunning, T. H. Jr. (1993). *J. Chem. Phys.*, **99**, 8774.
[14] Mò, O., Yàñez, M. and Elguero, J. (1997). *J. Chem. Phys.*, **107**, 3592.
[15] Szczesniak, M. M., Kendall, R. A. and Chalasinski, G. (1991). *J. Chem. Phys.*, **95**, 5169.
[16] N-H—N and N-H—O interactions are shown from the analysis of experimental IR spectra to correspond to very distorted HB structures in the ammonia homo dimer and the (H_2O, NH_3) hetero dimer (their X-H—Y angles are of 150 and 170°, respectively). Hence, it is questionable to characterize the latter interactions using the HB concept.
[17] Chalasinski, G., Szczesniak, M. M., Cieplak, P. and Scheiner, S. (1991). *J. Chem. Phys.*, **94**, 23.

[18] Ahlström, P., Wallqvist, A., Engström, S. and Bo. Jönsson (1989). *Mol. Phys.*, **68**, 563.
[19] Hodges, M. P., Stone, A. J. and Xantheas, S. (1997). *J. Phys. Chem. A*, **101**, 9163.
[20] Gresh, N. (1997). *J. Phys. Chem. A*, **101**, 8680.
[21] Coulson, C. A. (1957). *Res. Appl. Ind.*, **10**, 149.
[22] Isaacs, E. D., Shukla, A., Platzman, P. M., Hamann, D. R., Barbielline, B. and Tulk, C. A. (1999). *Phys. Rev. Lett.*, **82**, 600.
[23] Masella, M. and Flament, J.-P. (1997). *J. Chem. Phys.*, **107**, 9105.
[24] Masella, M. and Flament, J.-P. (1998). *Chem. Phys. Lett.*, **286**, 177.
[25] Mhin, B. J., Kim, J., Lee, J. Y. and Kim, K. S. (1994). *J. Chem. Phys.*, **100**, 4484; Kim, K., Jordan, K. D. and Zwier, T. S. (1994). *J. Am. Chem. Soc.*, **116**, 11568.
[26] Masella, M. (1998). *CR. Acad. Sci. IIc*, **1**, 441.
[27] Leforestier, C., Personnal communication.
[28] Masella, M. and Flament, J.-P. (1998). *Mol. Phys.*, **95**, 97.
[29] Okunbor, D. I. and Skeel, R. D. (1994). *J. Comput. Chem.*, **15**, 72.
[30] Masella, M. and Flament, J.-P. (1999). *J. Chem. Phys.*, **111**, 5081.
[31] Wales, D. J. and Ohmine, I. (1993). *J. Chem. Phys.*, **98**, 7245; Wales, D. J. and Ohmine, I. (1993). *J. Chem. Phys.*, **98**, 7257.
[32] Walfaren, G. E., Hokmabadi, M. S. and Yang, W.-H. (1986). *J. Chem. Phys.*, **85**, 6964.
[33] Libnau, F. O., Toft, J., Christy, A. A. and Kvalheim, O. M. (1994). *J. Am. Chem. Soc.*, **116**, 8311.
[34] Manivet, P. and Masella, M. (1998). *Chem. Phys. Lett.*, **288**, 642.